Vibrational modes in silicon clathrate compounds: A key to understanding superconductivity

E. Reny,[1] A. San-Miguel,[2] Y. Guyot,[3] B. Masenelli,[2] P. Mélinon,[2] L. Saviot,[3] S. Yamanaka,[1] B. Champagnon,[3] C. Cros,[4]
M. Pouchard,[4] M. Borowski,[5] and A. J. Dianoux[6,*]

[1]*Department of Applied Chemistry, Faculty of Engineering, Hiroshima University, Higashi-Hiroshima 739-8527, Japan*
[2]*Département de Physique des Matériaux UMR CNRS 5586, Université Claude Bernard-Lyon 1, 69622 Villeurbanne, France*
[3]*Laboratoire de Physico-Chimie des Matriaux Luminescents, UMR 5620, 69622 Villeurbanne, France*
[4]*Institut de Chimie de la Matière Condensée de Bordeaux, Université Bordeaux I, 33608 Pessac, France*
[5]*Institut Laue Langevin, BP 156, Grenoble Cedex 9, France*
[6]*E.S.R.F., BP 220, 38043 Grenoble, France*

Several doped type-I silicon clathrates ($Na_8@Si_{46}$, $K_8@Si_{46}$, $Ba_8@Si_{46}$ and $I_8@Si_{46}$) have been investigated both experimentally by inelastic neutron scattering and x-ray-absorption spectroscopy and theoretically by *ab initio* calculations. We find that Ba atoms have a stronger coupling with the host lattice than Na or K ones. We show that in the superconductor $Ba_8@Si_{46}$ the coupling is effectively done by host acoustic phonons exciting guest acoustic modes. These features suggest that the host-guest vibrational coupling is a crucial parameter to explain the appearance of superconductivity in addition to the density of states near the Fermi level.

I. INTRODUCTION

Type-I clathrates have a cage-type structure obtained by a face-shared assemblage of silicon polyhedra that form around guest atoms during the synthesis.[1] Column-IV (Si, Ge, Sn, and hypothetical C) clathrates are attracting much attention because of their superconducting,[2] wide-gap,[3–6] thermoelectric,[7,8] or ultrahard[9,10] properties. The type-I silicon clathrate lattice is an arrangement of two pentagonal dodecahedra (Si_{20}) and six tetrakaidecahedra (Si_{24}) offering eight sites per unit cell for guest alkali, alkaline-earth or even, as reported very recently, halogen atoms (M).[11] The resulting formula is therefore $(M@Si_{20})_2(M@Si_{24})_6Si_{46}$ or for the sake of simplification $M_8@Si_{46}$. In particular, endohedrally Ba-doped silicon clathrates of the type I constitute the only known sp^3 silicon based material superconductor at normal pressure. In fact, superconductivity has been reported for $Ba_8@Si_{46}$,[12] $Na_xBa_{8-x}@Si_{46}$,[2] $Ba_8@[Ga_{16}Ge_{30}]$,[13] and $Ba_8@[TM_xSi_{46-x}]$ (TM = Au, Ag, Cu)(Ref. 14) clathrates with a maximum T_c of 8 K for $Ba_8@Si_{46}$. Their superconductivity mechanism is still disputed. Some authors propose a phonon-mediated Bardeen-Cooper-Schrieffer (BCS) mechanism as observed in doped fullerenes.[15] According to this, T_c depends on two terms, the density of states (DOS) at the Fermi level $N(E_F)$ and the electron-phonon coupling factor. Recent measurements[16] show that $Ba_8@Si_{46}$ has a type-II superconductivity behavior, while $Na_8@Si_{46}$ has no superconductivity. Some theoretical predictions give a higher $N(E_F)$ in $Ba_8@Si_{46}$ than in $Na_8@Si_{46}$.[17] This is understood as an hybridization effect: Ba_{5d} orbitals are more hybridized with silicon than Na_{3s} states.[5,17] Nevertheless, this results raise the problem of the total absence of superconductivity in $Na_8@Si_{46}$ for which $N(E_F) \neq 0$.[18] This paper reports insight in the understanding of the parameters that govern the superconductivity in such materials, especially the coupling between the guest atom

and the host lattice. For this purpose, we characterize the coupling modes between a guest atom (Na, K,Ba, and I) and the silicon host (Si_{20} or Si_{24} cage) both by inelastic neutron scattering, extended x-ray-absorption fine structure (EXAFS) spectroscopy and *ab initio* calculations. We experimentally show the increase of the hybridization inside the series Na, K, Ba, and I guest atoms. We also find a correlation between the disappearance of the guest atom localized mode and the appearance of the superconductivity. All the experiments are in good agreement with our calculations on these systems.

II. EXPERIMENTAL PROCEDURE

Different means have been used for the elaboration of each sample. $Na_8@Si_{46}$ was prepared by thermal decomposition of the Zintl phase NaSi under argon flow at 680 K.[19] $K_8@Si_{46}$ was obtained by pyrolysis of KSi under secondary vacuum.[20] For $Ba_8@Si_{46}$ and $I_8@Si_{46-x}I_x$, high-pressure high-temperature (HPHT) conditions are required.[12,11] The inelastic neutron-scattering experiments were carried out at the Institut Laue Langevin in Grenoble on the IN6 beam line, equipped with a time-of-flight spectrometer. The incident wavelength was 4.12 Å and the momentum transfer ranged between 0.39 and 2.56 Å^{-1}. The incident neutron beam, extracted by a triple monochromator crystal assembly, was time focused by a Fermi chopper. The time-of-flight path was 248 cm in length with an angle range from 10° up to 114°. The detection was performed using 337 elliptical ^{3}He detectors. Some corrections were applied on the obtained spectra in order to take into account the background and aluminum cell contributions. An integration over the full angular range resulted in obtaining an incoherent approximation of a phonon DOS.[21] All the samples are fine powders (about 300 mesh), pressed between two aluminum foils. For the superconductor Ba_8Si_{46}, EXAFS was performed at the BM29 beamline of the European Synchrotron Radiation Facility (ESRF, Grenoble, France) with a Si (111) helium cooled
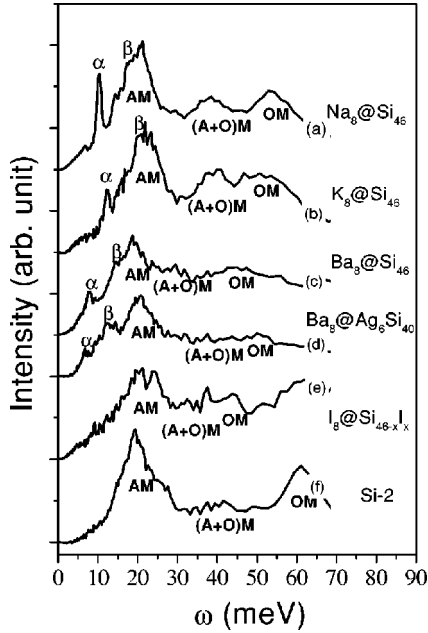
FIG. 1. Inelastic-scattering data determined at 300 K of various silicon clathrates (a)–(e) and pure silicon (f). α and β design the low-frequency molecular modes (mmf) corresponding to the rattling of the entrapped atoms in the cages. AM, OM, and $(A+O)M$ stand, respectively, for acoustic modes, optic ones, and the mixed contribution of the two.

double crystal monochromator working at 50% detuning for harmonic reduction. Samples were placed in a He DISPLEX cryostat and transmission spectra at the Ba K edge were recorded at three different temperatures, namely 20, 100, and 300 K. Three different scans were recorded at each temperature and then averaged. Measurements at low temperature are essential for the correct interpretation of the spectra since the Ba-Si and Ba-Ba coupling factors are weak leading to a large thermal damping of the signal.

III. RESULTS

A. Inelastic neutron scattering

Inelastic neutron scattering can provide a quantitative measure of the phonon density of states (PDOS) of a solid as a function of energy. In general to obtain the PDOS from inelastic neutron-scattering data in a multielement solid needs the introduction of a detailed model of the lattice dynamics. Nevertheless, quantitative information can be extracted if, for instance, the different atomic species participate in totally decoupled vibrational modes. In Fig. 1 are depicted the inelastic-scattering data determined at 300 K for $Na_8@Si_{46}$ (a), $K_8@Si_{46}$ (b), $Ba_8@Si_{46}$ (c), $Ba_8@Ag_6Si_{40}$ (d) $I_8@Si_{46-x}I_x$ (e), and silicon diamond Si-2 (f).

Some of the features of spectra (a), (b), and (f) have been already reported: the influence of the multiphonon processes are negligible and the low intensity of the transverse optical-like bands (OM) with respect to the transverse acousticlike ones could be assigned to the finite value of the momentum transfer.[22] As our data have been collected on the same apparatus, in the same conditions, it is reasonable to assume

that these conclusions can be extended to spectra (c), (d), and (e). For all samples except $I_8@Si$-46 where the signal-to-noise ratio is poor, three regions could be easily defined and attributed to AM (acoustic modes), $(A+O)M$ and OM.[22] We note that the terms "optical" and "acoustic" modes are used as a matter of convenience to allow comparison between samples. Actually these terms are defined for specific wave vectors and not for a range of energy. Moreover, the nonparity of pentagonal rings leads to a lattice frustration preventing establishment of purely optical vibrations. For all silicon clathrates doped with electropositive elements, i.e., corresponding to spectra (a)–(c), we notice two narrow low-energy molecular modes (Einstein modes) that are attributed to the rattling of the trapped atoms in the two types of cages similarly to what has been observed in filled skutterudite antimonides structures.[23] In each spectrum, the low-energy mode, α is assigned to the rattling in the largest cage Si_{24} and the higher one, β to rattling of the guest atom in the Si_{20} cage. We will refer to these modes as guest molecular modes frequencies (mmf). The obtained values are reported in Table I. For the Na, K, and Ba intercalated clathrates, the α (Si_{24}) mmf is defined enough to admit a good Lorentzian fitting. The full width at half maximum (FWHM) obtained is reported in Table II. It clearly appears that in the Si_{24} cages the Ba atoms have a stronger coupling with the host structure than the alkali ones.[23] We have also reported in this table the coherent scattering length of the guest atoms refereed to the silicon one. Here again we observe that for an equal coupling the Ba and I atoms should present higher intensity mmf's than the alkali ones. All guest atoms in the Si_{20} cages are strongly coupled with the host lattice.

B. EXAFS

The Ba K-edge EXAFS oscillations were extracted from the absorption spectra with the standard AUTOBK procedure.[24] Figure 2 displays the EXAFS of Ba_8Si_{46} at the Ba K-edge at $T=20$, 100, and 300 K. The Fourier transform of the experimental EXAFS signal is shown in Fig. 3. EXAFS oscillations were expressed in terms of the photoelectron wave number $k=1/[\hbar\sqrt{2m(E-E_0)}]$ where m is the electron mass and E_0 is chosen at the inflexion point of the threshold and further adjusted in the fitting procedure.

For a given position of the Ba atom in the cages, we can compute single- and multiple-scattering paths contributing to the EXAFS signal and adjust some fitting parameters using the FEFFIT code[25] to try to match the experimental spectra. The contributions of single- and multiple-scattering paths to the EXAFS signal are calculated within the framework of *ab initio* self-consistent real-space multiple-scattering FEFF8 code.[26] In this formalism the total EXAFS signal $\chi(k)$ writes

$$\chi(k)=\sum_\Gamma \chi_\Gamma(k), \qquad (1)$$

where $\chi_\Gamma(k)$ is the contribution to the signal of each considered single- or multiple-scattering path Γ. This contribution is evaluated as[25]

TABLE I. Si modes, guest atom molecular modes frequencies (mmf's), and K factor coupling in the harmonic oscillator framework. Calculations have been performed considering the displacement of the guest atoms towards the center of a pentagon (cp) or an hexagon (ch) or towards the atom of a pentagon (ap) or an hexagon (ah).

	$Na_8@Si_{46}$	$K_8@Si_{46}$	$Ba_8@Si_{46}$
mmf (neutrons) in Si_{20} [a]	18±1	20.0±0.5	14.4±0.5
mmf (x-ray diffraction) in Si_{20}	23 [b]		12.7 [c]
mmf(calculated) in Si_{20} (cp)	18.8		14.6
mmf (neutrons) in Si_{24} [a]	10.3±0.2	12.2±0.2	7.8±0.2
mmf (x-ray diffraction) in Si_{24}	15.9 [b]		8.0 [c]
mmf (calculated) in Si_{24} (ap,ah,cp,ch)	8.4, 9.6, 10.3,12.9		8.6, 9.2, 8.9, 10.6
K_{exp} in Si_{20}(neutrons) [d]	1.8±0.2	3.8±0.2	7.0±0.5
K_{th} in Si_{20}(cp) [d]	1.8		7.1
K'_{th} in Si_{20}(cp) [e]	1.32		3.68
K_{exp} in Si_{24}(neutrons) [d]	0.60±0.03	1.48±0.05	2.1±0.1
K_{th} in Si_{24}(ap,ah,cp,ch) [d]	0.40, 0.52, 0.6, 0.94		2.50, 2.88, 2.9, 3.8
K'_{th} in Si_{24}(ap,ah,cp,ch) [e]	0.4, 1.16, 0.64, 0.36		1.24, 3.68, 2.4, 1.68

[a]mmf in meV.
[b]From Ref. 37.
[c]From Ref. 29.

[d]K in eV/$Å^2$
[e]K' in eV/$Å^4$

$$\chi_\Gamma(k) = \mathrm{Im}\left[\frac{N_\Gamma S_0^2 F_\Gamma(k)}{2kR_\Gamma^2} e^{i[2kR_\Gamma + \Phi_\Gamma(k)]} e^{-2k^2\sigma_\Gamma^2} \right], \quad (2)$$

where N_Γ is the degeneracy of the path, S_0^2 is the passive electron reduction factor, R_Γ is the length of the path, and σ_Γ^2 is the root-mean-square displacement of the path length. The effective backscattering amplitude $F_\Gamma(k)$ and phase shift $\Phi_\Gamma(k)$ are computed by FEFF.

We consider all the photoelectron scattering paths having as origin the barium atoms and with a maximum half scattering length of 7 Å. Depending on the considered position of the Ba atom inside the Si_{24} and Si_{20} cages, up to 100 different scattering paths had to be considered. We have checked that the number of pathways is significant enough so that the truncation of the sum in Eq. (1) has converged to the real EXAFS signal.

In a previous work,[27] we showed that the equilibrium position of the sodium atoms is out of the center of the Si_{28} cage in a type-II silicon clathrate. The displacement, that can be viewed as a strong Jahn-Teller effect, was about 1 Å in-

TABLE II. FWHM of the mmf corresponding to the guest atom in Si_{24} and guest coherent neutron scattering length normalized to the silicon one.

	FWHM (meV)	b/b_{Si}
Na	1.3±0.1	0.87
K	1.3±0.3	0.88
Ba	2.3±0.3	1.22
I		1.48

dicating a weak coupling. Such behavior has been also theoretically predicted in alloyed germanium clathrates,[28] even though no data are yet reported for Si_{24} cages.

The signal between 2 and 4 Å in Fig. 3 corresponds to the contribution of single-scattering paths involving the barium atom and the silicon ones of the Si_{20} and the Si_{24} cages. We have first fitted the corresponding filtered signal using as
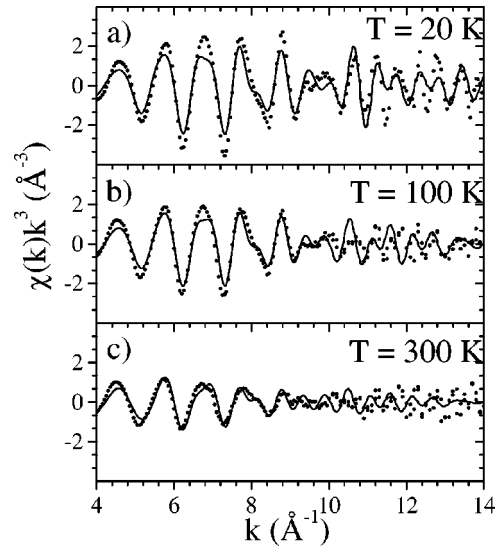

FIG. 2. Dots: Experimental EXAFS oscillations of Ba_8Si_{46} at the Ba K-edge at $T=20$, 100, and 300 K. The signal has been multiplied by k^3. Lines: corresponding fit of the data obtained with the Ba atoms placed at the center of the cages (see text for details). We note that at 300 K, the noise level dominates the signal for k values higher than 10 $Å^{-1}$
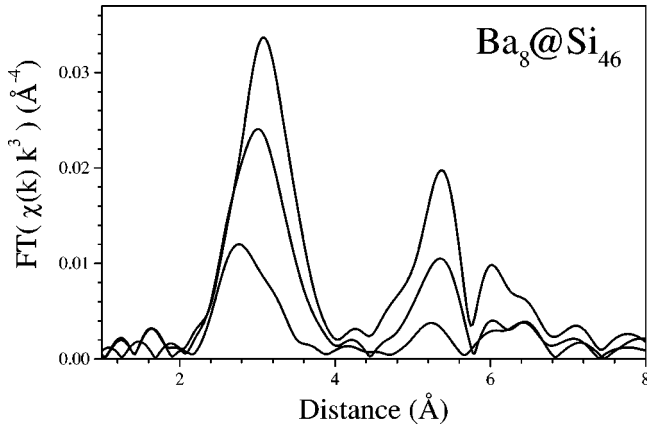
FIG. 3. Fourier transform of the EXAFS signal at $T = 20$, 100, and 300 K. The signal amplitude decreases with the temperature.

model structure the one obtained by x-ray diffraction[29] but allowing the out of center displacement of the barium atom. Our best fit was obtained considering Ba atoms at the center of both the Si_{20} and the Si_{24} cages. This fit allows as well to correct the phase-shift origin given by the FEFF code for Ba-Si paths. We find a correction of -1.5 eV that we used in the following analysis. We have then simultaneously fitted the EXAFS signal of the three spectra at 20, 100, and 300 K, considering the Einstein model for the dynamics of the inter-atomic distance, with a different Einstein temperature θ for the average Si-Ba single-scattering path for each type of cage. The fits shown in Figs. 2(a)–2(c) give $\theta_{20}^{Ba-Si} = 350 \pm 100$ K and $\theta_{24}^{Ba-Si} = 260 \pm 40$ K with associated energies of $E_{20}^{Ba-Si} = 30 \pm 9$ meV and $E_{24}^{Ba-Si} = 22 \pm 4$ meV.

The total experimental EXAFS signal at 20 K between 4 and 14 Å^{-1} was then fitted. The result is shown in panel (a) of Fig. 4. Here we have considered a total of 44 scattering paths. The different contributions to the total signal are shown in panels (b)–(e) of Fig. 4. We observe that the addition of the signals produces a strong "beating" at about 9.5 Å^{-1} in excellent agreement with the experiment as shown in Fig. 4(a). Phase shifts between the different components contributing to the EXAFS signal appear by displacing one of the Ba atoms, and immediately shift the beating position or give rise to its disappearance. *We claim that barium occupy exactly the center of the cages at low temperature.* We note also the importance of the Ba-Ba scattering paths at high k where its amplitude is comparable to the total multiple-scattering signal. In our EXAFS model, the only fitted parameters were the harmonic thermal characteristic of Ba-Ba scattering paths, the corresponding shift of E_0 (that was found to be zero), and an associated thermal term for the multiple-scattering paths. The Einstein temperature associated to the Ba-Ba correlations is of $\theta_{Ba-Ba} = 90 \pm 50$ K, or its associated energy, $E_{Ba-Ba} 8 \pm 5$ meV. The sensitivity of EXAFS to the factors affecting the amplitude of the $\chi(k)$ oscillations is much smaller than those affecting the phase of the signal. This explains the lower accuracy of the EXAFS mmf values when compared to neutrons.

C. *Ab initio* calculations

There are few *ab initio* calculations on the lattice vibrations of silicon clathrates.[30] Our *ab initio* calculations were
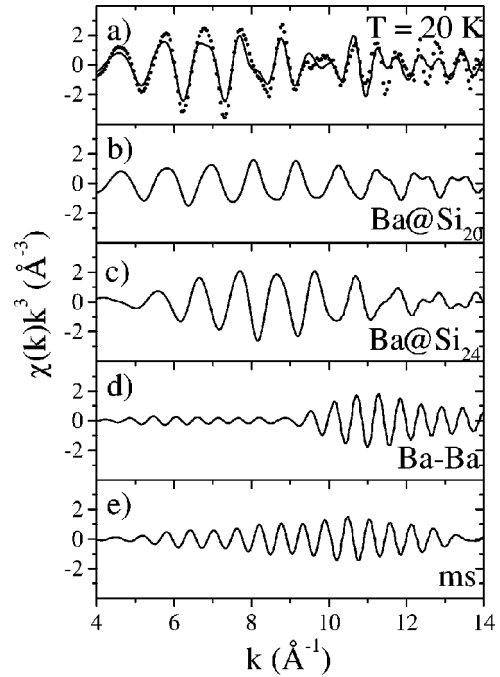

FIG. 4. (a)Experimental EXAFS oscillations at 20 K (dots) and best fit (continuous line) obtained with the Ba atoms placed at the center of the cages. The following panels show a decomposition of the signal that includes: (b) single-scattering paths having as origin the $Ba@Si_{20}$; (c) single-scattering paths having as origin the $Ba@Si_{24}$; (d) Ba-Ba single-scattering paths; (e) all multiple-scattering paths.

performed within the local-density approximation.[31,32] We adopt a pseudopotential approach[33,34] and a numerical-atomic-orbitals (NAO) expansion of the wave functions[35] using the SIESTA code.[36] We calculated the potential energy curves of guests by displacing a single guest atom (Na, Ba) in one of the cages (Si_{20} or Si_{24}) while keeping all other guest atoms fixed.

For Si_{20} we have computed the energy curve when the guest atoms (Na, Ba) are displaced towards the center of one pentagon or towards a silicon atom. For Si_{24} we have computed the energy curves with four configurations corresponding to displacements toward (i) the center of an hexagon or (ii) a pentagon or towards (iii) an atom of an hexagon or (iv) an atom shared only by pentagons. The fitting parameters of guest-framework interaction energy potentials is written as $E(x) = \frac{1}{2}Kx^2 + \frac{1}{4}K'x^4$. All the results are summarized in Table I together with the experimental data.

Our calculations show that there exist an anisotropy of rattling of the guest atoms inside the Si_{24} cages, characterized by vibrations that are softer in the direction of the atoms of the cage and harder when moving towards the center of the polyhedra. If we can quantify the degree of calculated anisotropy as the maximum of the difference between the different projections of the atomic movement, it appears that the anisotropy for the Ba atom is about 20%, half the one of Na atoms.

IV. DISCUSSION AND CONCLUSION

The comparison between the calculated and experimental values of the guest molecular modes frequencies (mmf)

shown in Table I should take into account the anisotropy of the guest atom movement evidenced by our calculations. The inelastic neutron-scattering as well as the x-ray-diffraction data[29,37] correspond to the time averaged value of the calculated mmf in the different directions.

The EXAFS atomic displacement parameters obtained for a single-scattering path between atoms X and Y, σ^2_{X-Y}, is to be related with the corresponding atomic displacements u_X and u_Y:

$$\sigma^2_{X-Y} = \langle (u_X - u_Y)^2 \rangle = \langle u_X^2 \rangle + \langle u_Y^2 \rangle - 2\langle u_X u_Y \rangle$$
$$= \langle u_X^2 \rangle + \langle u_Y^2 \rangle - 2\sqrt{\langle u_X^2 \rangle \langle u_Y^2 \rangle}\,\Phi. \quad (3)$$

Here Φ is a parameter measuring the degree of correlation between the displacements of X and Y atoms. Φ will be zero for totally decorrelated pairs of atoms, $\Phi = 1$ in the case of acoustic coupling, and $\Phi = -1$ for optical coupling.

The EXAFS value when considering the Ba-Ba scattering paths corresponds to an average of the mmf in the direction of the faces of the polyhedra (the direction of the Ba-Ba neighbors). On the other side when considering EXAFS single-scattering Ba-Si paths inside the cages we shall take into consideration the directions towards the silicon atoms.

For the weakly coupled Na atom, neutron and calculations agree remarkably well when considering the displacement towards the center of the pentagons, both in the Si_{20} and Si_{24} cage. In the Si_{24} cages of $Na_8@Si_{46}$, the calculated average mmf gives also a value of 10.3 eV (the same as that in the direction of the pentagons). The mmf projection in the Na-Si direction is about 20% smaller than the average value given by the neutron or the x-ray-diffraction experiments.

For $Ba_8@Si_{46}$, neutron and x-ray-diffraction data agree remarkably well. On the contrary, the calculated mmf seems to slightly overestimate the result from the neutron inelastic-scattering experiment. This could be a signature of a stronger coupling but can also be associated with defects in the Ba pseudopotential. Nevertheless, as already discussed, calculations show that the anisotropy in the thermal displacement of the Ba atom is half the one for the Na case. Consequently, we should consider a reduction of 10% of the average values of neutron or diffraction experiments to obtain the projection in the direction of silicon atoms and confront this values with the EXAFS ones through Eq. (3). As we do not know how silicon displacements are projected, in order to obtain an estimate of Φ, we will consider directly the values of neutron and diffraction experiments and add an additional 20% in the error estimation. Remarkably enough, the obtained coupling constants summarizing those calculations are the same for Ba-Si in both type of cages: $\Phi^{Ba-Si}_{Si_{20}} = \Phi^{Ba-Si}_{Si_{24}} = -0.35 \pm 0.1$.

Let us now consider the Ba-Ba scattering paths. More than 90% of the Ba-Ba next-nearest neighbors in the $Ba@Si_{46}$ structure are between Ba atoms in the Si_{20} and Ba atoms in the Si_{24} cages. The corresponding EXAFS signal contribution should then be mainly characterized by the average of both cages mmf in the direction of the center of the polyhedra. As we have seen for the Na case, the mmf signal towards the center of the pentagons can be considered as

representative of the average mmf. We can then directly consider the x-ray-diffraction or neutron values without modification and use Eq. (3) that gives $\Phi^{Ba-Ba} = 0.4 \pm 0.2$.

It is remarkable that the absolute value of the three coupling constants are equivalent, and that the sign of Φ^{Ba-Ba} is opposed to the one of the Ba-Si. We conclude that the Ba atoms are acoustically coupled between them through optical Ba-Si coupling. *This corresponds to the coupling of host acoustic modes with guest acoustic excitations.*

The energy of the molecular mode frequencies (mmf's) will depend on the mass of the guest, and on the overlapping between electron valence shell of the guest atom and the Si_{3s-3p} electrons. This last term will be a function of the ratio of the cage, the guest atom radius, and on the energy difference of the atomic energy levels. Assuming a classical harmonic oscillator, one easily observes that the coupling factor K_{exp} increases in the series Na, K, to Ba. This is also correlated to the softness of the Si stretching modes, clearly showing that the hybridization becomes more and more efficient from Na to Ba. The softening of the Si modes coincides with the electron transfer in the conduction band. This is due to the increase of the electron clouding between Si atoms. The introduction of metallic atoms in the host network ($Ba_8@Ag_6Si_{40}$) has clearly the effect of reducing the host-guest coupling.

The origin of the hybridization remains complex. For example, the extension of the Slater orbital for the guest atom plays an important role but do not explain entirely the coupling strength. We notice that the ionic radius is 0.95 Å in sodium and about 1.34 Å for potassium and barium while barium is more coupled than potassium (see below). For iodine, we found an acceptor state.[38] Iodine radii ranges between the neutral radius (1.4 Å) and the Pauling ionic radius 2.16 Å (in I^- state): this is the more coupled system. Nevertheless, a more efficient hybridization alone does not explain the superconductivity. As mentioned above the difference in ionization potentials between the guest and the host atom is a crucial parameter. Soft x-ray emission spectroscopy has been applied in order to visualize the electronic density of states at the Fermi level.[39] The experimental e-DOS showed a sharp peak at E_F for both the nonsuperconductor $Na_8@Si_{46}$ and superconductor $Ba_8@Si_{46}$.

In order to study the second term in the BCS theory, i.e., the electron-phonon coupling, it is of high importance to notice that the lowest energy molecular mode has been predicted by Yoshizawa *et al.*[40] This group argues that the Jahn-Teller distortion correlated with the superconductivity is due to the low-frequency phonon close to 12 meV in Si_{20}, this polyhedra having the strongest vibronic coupling constant. We actually observe this low-frequency phonon and it is therefore of high interest to compare its energy with the superconducting properties of each of the samples. All the mmf's range around 12 meV (see Table I). An efficient electron coupling involves a strong coupling between the guest atom vibration mode and the silicon cage. As a consequence, with an increasing coupling, the mmf must progressively broaden, to finally disappear in the phonon density of states, i.e., the amplitude of the mmf is inversely proportional to the K coupling factor. We observe in Fig. 1 that the mmf modes

corresponding to Si_{20} cages have a weak intensity independently of the nature of the guest atom. The electron-phonon coupling can be efficient in such cages. However, the mmf corresponding to Si_{24} cages has a high intensity in sodium and decreases strongly in barium (potassium being an intermediate case) inspite of the higher coherent neutron-scattering factor of Ba. We also observe in Table II that the FWHM of the Ba mmf in the Si_{24} cages is almost two times the one of Na or K. Therefore sodium or potassium are weakly coupled to the Si_{24} cage while barium atoms show a much stronger coupling. This could be correlated to the occurrence of the superconductivity in $Ba_8@Si_{46}$. In fact, EX-AFS shows that the Ba atom in $Ba_8@Si_{46}$ is well localized in the cage center and phonon-coupled to the silicon network. Contrarily, in $Na_8@Si_{46}$ a strong anharmonicity due to the Na guest has been theoretically predicted at low temperatures[41] that is associated with the rattling of the guest atom. Our neutron inelastic-scattering data and calculations (that as shown in Table I give an average k'/k that is bigger in the Na that in the Ba case) are compatible with such prediction. This type of anharmonicity will not be favorable to the dynamic guest-host coupling necessary for the superconducting behavior.

We observe the highest coupling in the iodine case since no mmf is observed. Unfortunately, the strong expected electron-phonon coupling is counterbalanced by a zero density at the Fermi level:[39] $I_8@Si_{46}$ is not a superconductor. We note here that in recent *ab initio* calculations[38] it was reported a density of states with a Fermi level of $I_8@Si_{46}$ located just beneath the top of the valence band. Nevertheless, this prediction does not correspond to the real stoichiometry of the iodine intercalated clathrate that is more complex (see the introduction) and conductivity measurements report an insulating state. We can then expect that the Fermi level just coincides with the top of the valence band. The case of $Ba_8@Ag_6Si_{40}$ is more difficult to discuss due to the lack of data on the electronic density of states.

In conclusion, we have reported the experimental evidence of the coupling between the guest atom and the cage host through host acoustic modes. Such coupling was deduced from both the phonon DOS and the vibrational motion measured by inelastic neutron-scattering and EXAFS spectroscopy. We found that the main parameters to be correlated to the superconductor properties are the host-guest vibrational coupling inside the Si_{24} cage and the density of states at the Fermi level. Coupling inside the Si_{24} cages is essential to obtain the acoustic excitation of the Ba subnetwork. It appears that the enhancement of the critical temperature needs a large ionic radius for the donor atom in the Si_{24} cage while no such condition is required for donor atoms located in Si_{20} cages where the coupling is already strong.

*Email address: sanmigue@dpm.univ-lyon1.fr

[1] C. Cros, M. Pouchard, and P. Hagenmuller, C. R. Hebd. Seances Acad. Sci. **260**, 4764 (1965).

[2] H. Kawaji, H. omi Horie, S. Yamanaka, and M. Ishikawa, Phys. Rev. Lett. **74**, 1427 (1995).

[3] A. Demkov, O. Sankey, K. Schmidt, G. Adams, and M. Keefe, Phys. Rev. B **50**, 17 001 (1994).

[4] G. Adams, M. O'Keeffe, A. Demkov, O. Sankey, and Y.M. Huang, Phys. Rev. B **49**, 8048 (1994).

[5] S. Saito and A. Oshiyama, Phys. Rev. B **51**, 2628 (1995).

[6] J. Gryko, P.F. McMillan, R.F. Marzke, G.K. Ramachandran, D. Patton, S.K. Deb, and O.F. Sankey, Phys. Rev. B **62**, 7707 (2000).

[7] G. Nolas, T. Weakley, J. Cohn, and R. Sharma, Phys. Rev. B **61**, 3845 (2000).

[8] J. Dong, O. Sankey, and C.W. Myles, Phys. Rev. B **86**, 2361 (2001).

[9] A. San-Miguel, P. Kéghélian, X. Blase, P. Mélinon, A. Perez, J. Itié, A. Polian, E. Reny, C. Cros, and M. Pouchard, Phys. Rev. Lett. **83**, 5290 (1999).

[10] A. San-Miguel, P. Mélinon, D. Connetable, X. Blase, F. Tournus, E. Reny, S. Yamanaka, and J. Itié, Phys. Rev. B **65**, 054109 (2002).

[11] E. Reny, S. Yamanaka, C. Cros, and M. Pouchard, Chem. Commun. (Cambridge) **24**, 2505 (2000).

[12] S. Yamanaka, E. Enishi, H. Fukuoka, and M. Yasukawa, Inorg. Chem. **39**, 56 (2000).

[13] J. Bryan, V. Srdanov, G. Stucky, and D. Schmidt, Phys. Rev. B **60**, 3064 (2000).

[14] R. Herrmann, K. Tanigaki, S. Kuroshima, and H. Suematsu, Chem. Phys. Lett. **282**, 29 (1998).

[15] R. Fleming, A. Ramirez, M. Rosseinsky, D. Murphy, R. Haddon, S.M. Zahurak, and A. Makhija, Nature (London) **352**, 787 (1991).

[16] I.M. Gat, Y. Fudamoto, A. Kinkhabwala, M.I. Larkin, G.M. Luke, J. Merrin, B. Nachumi, Y.J. Uemura, K.M. Kojima, E. Eiji, and S. Yamanaka, Physica B **289-290**, 385 (2000).

[17] K. Moriguchi, M. Yonemura, A. Shintani, and S. Yamanaka, Phys. Rev. B **61**, 9859 (2000).

[18] J. Gryko, P. McMillan, R. Marzke, A. Dodokin, A. Demkov, and O. Sankey, Phys. Rev. B **57**, 4172 (1998).

[19] C. Cros, M. Pouchard, and P. Hagenmuller, J. Solid State Chem. **2**, 570 (1970).

[20] C. Cros, M. Pouchard, P. Hagenmuller, and J. Kasper, Bull. Soc. Chim. Fr. **7**, 2737 (1968).

[21] A. Fontana, F. Rocca, M. Fontana, B. Rosi, and A. Dianoux, Phys. Rev. B **41**, 3778 (1990).

[22] P. Melinon, P. Keghelian, A. Perez, B. Champagnon, Y. Guyot, L. Saviot, E. Reny, C. Cros, M. Pouchard, and A.J. Dianoux, Phys. Rev. B **59**, 10 099 (1998).

[23] V. Keppens, D. Mandrus, B. Sales, B. Chakoumakos, P. Daia, R. Coldes, M. Maple, D. Gajewski, E.J. Freeman, and S. Bennington, Nature (London) **395**, 876 (1998).

[24] M. Newville, P. Livins, Y. Yacoby, E.A. Stern, and J.J. Rehr, Phys. Rev. B **47**, 14 126 (1993).

[25] M. Newville, B. Ravel, D.H. Askel, J.J. Rehr, E.A. Stern, and Y. Yacbi, Physica B **154**, 208 (1995).

[26] A.L. Ankudinov, B. Ravel, J.J. Rehr, and S.D. Conradson, Phys. Rev. B **68**, 7565 (1998).

[27] B.F. Brunet, P. Mélinon, A. San-Miguel, P. Kéghélian, A. Perez, A. Flank, E. Reny, C. Cros, and M. Pouchard, Phys. Rev. B **61**, 16 550 (2000).

[28] J. Dong, O.K.F. Sankey, G.K. Ramachandran, and P.F. McMillan, J. Appl. Phys. **87**, 7726 (2000).

[29] A. Kitano, K. Moriguchi, M. Yonemura, S. Munetoh, A. Shintani, H. Fukuoka, S. Yamanaka, E. Nishibori, M. Takata, and M. Sakata, Phys. Rev. B **68**, 045206 (2001).

[30] J. Dong, O. Sankey, and G. Kern, Phys. Rev. B **60**, 950 (1999).

[31] P. Hohenberg and W. Kohn, Phys. Rev. **136**, 864 (1964).

[32] W. Kohn and L.J. Sham, Phys. Rev. **140**, 1133 (1965).

[33] N. Troullier and J.L. Martins, Phys. Rev. B **43**, 1993 (1991).

[34] L. Kleinman and D.M. Bylander, Phys. Rev. Lett. **48**, 1425 (1982).

[35] D. Sánchez-Portal, E. Artacho, and J.M. Soler, J. Phys.: Condens. Matter **8**, 3859 (1996).

[36] D. Sánchez-Portal, P. Ordejón, E. Artacho, and J.M. Soler, Int. J. Quantum Chem. **65**, 453 (1997).

[37] E. Reny, P. Gravereau, C. Cros, and M. Pouchard, J. Mater. Chem. **8**, 2839 (1998).

[38] D. Connétable, V. Timoshevskii, E. Artacho, and X. Blase, Phys. Rev. Lett. **87**, 206405 (2001).

[39] K. Kobayashi, A. Fukushima, Y. Harada, T. Takeushi, S. Shibagaki, M. Watanabe, Y. Tanaka, K. Moriguchi, S. Munetoh, M. Yonemura, and S. Yamanaka, Annual Meeting of the Physical Society of Japan, 25-27/08/2000 (Japan) (2000).

[40] K. Yoshizawa, T. Kato, M. Tachibana, and T. Yamabe, J. Phys. Chem. **102**, 10 113 (1998).

[41] L. Qiu, M. White, Z. Li, J. Tse, C. Ratcliffe, C.A. Tulk, J. Dong, and O.F. Sankey, Phys. Rev. B **64**, 024303 (2001).